Article

Probing the Molecular Orbitals and Charge Redistribution in Organometallic (PP)Pd(XX) Complexes. A Pd K-Edge XANES Study

Moniek Tromp, Jeroen A. van Bokhoven, Gino P. F. van Strijdonck, Piet W. N. M. van Leeuwen, Diek C. Koningsberger, and David E. Ramaker

J. Am. Chem. Soc., **2005**, 127 (2), 777-789• DOI: 10.1021/ja048225n • Publication Date (Web): 23 December 2004

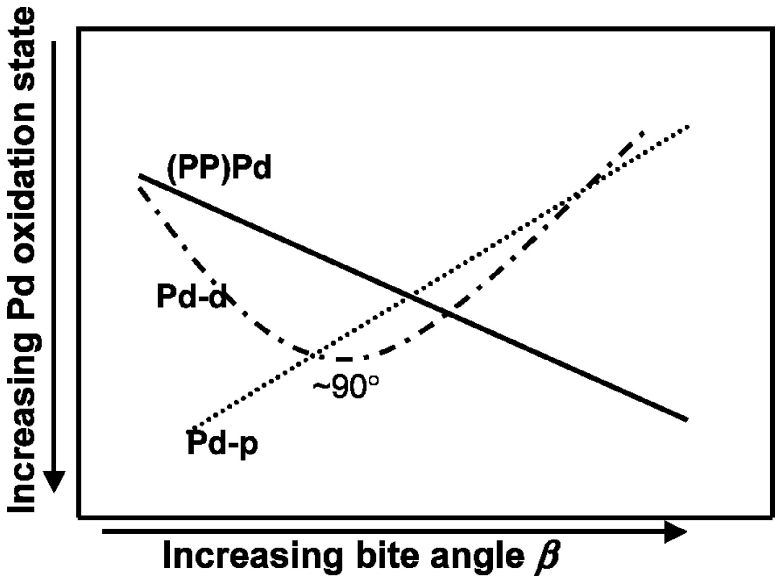

More About This Article

Additional resources and features associated with this article are available within the HTML version:

- Supporting Information
- Links to the 1 articles that cite this article, as of the time of this article download
- Access to high resolution figures
- Links to articles and content related to this article
- Copyright permission to reproduce figures and/or text from this article

View the Full Text HTML

J|A|C|S
ARTICLES
Published on Web 12/23/2004

Probing the Molecular Orbitals and Charge Redistribution in Organometallic (PP)Pd(XX) Complexes. A Pd K-Edge XANES Study

Moniek Tromp,[†] Jeroen A. van Bokhoven,[‡] Gino P. F. van Strijdonck,[§] Piet W. N. M. van Leeuwen,[§] Diek C. Koningsberger,[†] and David E. Ramaker*,[||]

Contribution from the Debye Institute, Department of Inorganic Chemistry and Catalysis, Utrecht University, Sorbonnelaan 16, 3584 CA Utrecht, The Netherlands, Institute for Chemical- and Bioengineering, Swiss Federal Institute of Technology (ETH Zurich), HCl E115, Zurich, Switzerland, Van't Hoff Institute for Molecular Sciences, University of Amsterdam, Nieuwe Achtergracht 166, 1018 WV Amsterdam, The Netherlands, and Department of Chemistry and Materials Science Institute, George Washington University, Washington, DC 20052

Received March 29, 2004; E-mail: ramaker@gwu.edu

Abstract: Pd K-edge X-ray absorption near-edge spectroscopy (XANES) is used to probe the unoccupied molecular orbitals in bidentate diphosphine Pd complexes. Complexes containing a series of bidentate diphosphine ligands (PP) are examined to study the effect of the ligand bite angle on the charge redistribution in these complexes. Different coordinating moieties (XX) have been used to induce a range of Pd oxidation states. A full interpretation of the Pd K-edge XANES data is presented. The negative second derivative of these XANES data provides direct information on the energy and electronic distribution of the different unoccupied molecular orbitals probed. The charge redistributions within the complexes, as reflected in the effective Pd oxidation state, are indicated by both the intensity of the first edge feature, the "Pd d peak", and the energy of the second edge feature, the "Pd p peak", which can be easily observed in the negative second derivative of the XANES data. Additionally, the changing covalent interaction between the Pd and coordinated moieties via the Pd p orbitals is reflected directly in the energy splitting of the "Pd p" peak. Thus, investigation of these (PP)Pd(XX) complexes, some used as catalysts in organic synthesis, with XANES spectroscopy provides new essential information on their electronic properties. Further, the XANES analysis techniques described in this paper can be applied to investigate the unoccupied molecular orbitals and charge redistributions within a wide range of samples.

Introduction

Palladium is one of the most widely used metals in transition-metal-catalyzed organic synthesis, as it is capable of catalyzing a wide variety of commercially important reactions.[1] Various ligands, most often phosphine ligands, are employed to tune the performance and increase the stability of the Pd catalysts. Changing the ligands enables fine-tuning of the steric and electronic properties of the catalyst and thereby the activity and selectivity of the catalyst.[2]

Bidentate diphosphine ligands are widely applied and their utility in homogeneous catalysts and metal complexes has been the subject of research for many years. An important ligand parameter to describe the bidentate diphosphine ligand (PP) complexes is the so-called bite angle β, that is, the P−M−P angle.[3,4] The natural preferred bite angle, β_n, of a bidentate diphosphine ligand can be calculated using molecular mechanics.[5] In this way, ligand bite angle trends can be deducted without the requirement of crystal structures. The P−Pd−P bite angles reported in this study (Table 1), however, are obtained from crystal structure analyses.

Several studies[2,3,4,6,7] discussed the ligand bite angle effect observed for different catalytic systems. The steric and electronic

[†] Utrecht University.
[‡] Swiss Federal Institute for Technology.
[§] University of Amsterdam.
[||] George Washington University.

(1) (a) Hegedus, L. *Transition Metals in the Synthesis of Organic Molecules*; University Science Books: Mill Valley, CA, 1994. (b) Trost, B. M.; van Franken, D. V. *Chem. Rev.* **1996**, *96*, 395.
(2) Tolman, C. A. *Chem. Rev.* **1977**, *77*, 31.
(3) van Leeuwen, P. W. N. M.; Kamer, P. C. J.; Reek, J. N. H.; Dierkes, P. *Chem. Rev.* **2000**, *100*, 2741.
(4) Dierkes, P.; van Leeuwen, P. W. N. M. *J. Chem. Soc., Dalton Trans.* **1999**, 1519.
(5) Casey, C. P.; Whiteker, G. T. *Isr. J. Chem.* **1990**, *30*, 299.
(6) Freixa, Z.; van Leeuwen, P. W. N. M. *J. Chem. Soc., Dalton Trans.* **2003**, 1890.
(7) (a) van Haaren, R. J.; Goubitz, K.; Fraanje, J.; van Strijdonck, G. P. F.; Oevering, H.; Coussens, B.; Reek, J. N. H.; Kamer, P. C. J.; van Leeuwen, P. W. N. M. *Inorg. Chem.* **2001**, *40*, 3363. (b) van Haaren, R. J.; Oevering, H.; Coussens, B.; van Strijdonck, G. P. F.; Reek, J. N. H.; Kamer, P. C. J.; van Leeuwen, P. W. N. M. *Eur. J. Inorg. Chem.* **1999**, 1237. (c) Sjorgen, M. P. T.; Hansson, S.; Åkermark, B.; Vitagliano, A. *Organometallics* **1994**, *13*, 1963. (d) van Haaren, R. J.; Druijven, C. J. M.; van Strijdonck, G. P. F.; Oevering, H.; Reek, J. N. H.; Kamer, P. J. C.; van Leeuwen, P. W. N. M. *J. Chem. Soc., Dalton Trans.* **2000**, *10*, 1549.

Table 1. Bite Angles for Series of (PP)Pd(XX) Complexes

complex	β (°)	complex	β (°)
(dppe)Pd(TCNE)	82.55(3.65)[a]	(dppe)Pd(C_3H_5)	85.77[d]
(dppf)Pd(TCNE)	98.74(3.42)[a]	(dppp)Pd(C_3H_5)	95[d]
(DPEphos)Pd(TCNE)	101.46(3)[b]	(DPEphos)Pd(C_3H_5)	99[d]
(Xantphos)Pd(TCNE)	101.64(5)[b]	(Xantphos)Pd(C_3H_5)	108.11(7)[e]
		(dppe)Pd(C_5H_9)	85.77[e]
		(dppp)Pd(C_5H_9)	95[e]
(dppe)PdCl_2	85.8[c]	(dppb)Pd(C_5H_9)	99[e]
(dppf)PdCl_2	99.07[c]	(dppf)Pd(C_5H_9)	101.2(3)[e]
(DPEphos)PdCl_2	101.46[a]	(DPEphos) Pd(C_5H_9)	103.93(6)[e]
(Xantphos)PdCl_2	101.64[a]	(Xantphos) Pd(C_5H_9)	108.11(7)[e]

[a] Estimated on the basis of ref 4. Numbers in parentheses indicate uncertainty in angle [b] Reference 13. [c] Reference 14. [d] Taken as C_5H_9. [e] Reference 7a.

changes after ligand modification are investigated and different effects are suggested to be important for different reactions. For example, large differences in regioselectivity with bite angle were observed in the allylic alkylation reaction using (PP)Pd catalysts. Therefore, the $[(PP)Pd(allyl)]^+$ reaction intermediates have been isolated and characterized in detail to gain more insight into the observed activity and selectivity of these catalysts.[7] The $[(PP)Pd(allyl)]^+$ complexes have been studied by molecular modeling, X-ray crystallography, (solution-) NMR, and EXAFS techniques to obtain information on their steric and electronic properties.[7,8] Additionally, a series of theoretical papers modeling these complexes have appeared proposing orbital interaction diagrams and discussing the influence of ligand modification and consequent catalytic properties.[9]

To gain more detailed electronic information on different (PP)Pd complexes, we have applied X-ray absorption fine structure (XAFS) spectroscopy. XAFS spectroscopy is capable of providing structural and electronic information about a specific element in a compound in any state of aggregation.[10] In this manuscript, we will focus on the electronic properties of the (PP)Pd complexes by performing a detailed X-ray absorption near-edge spectroscopy (XANES) study.

Detailed XANES studies have been described in the literature previously for transition-metal complexes showing that the X-ray absorption edges are very sensitive to the chemical environment.[11] Moreover, the preedge is indicative of different oxidation states and geometry of the samples under investigation.[11] For metals such as palladium and rhodium, the K edge is observed at high energies (the Pd K edge at 24350 eV), showing a very broad and seemingly nondescript edge, in part because of the large 1s core-level width which broadens the spectrum even with high experimental resolution. Perhaps for this reason, no detailed studies on these edges have been reported, at least to our knowledge.

Scheme 1. Overview of the (PP)Pd(XX) Complexes Used in This Study

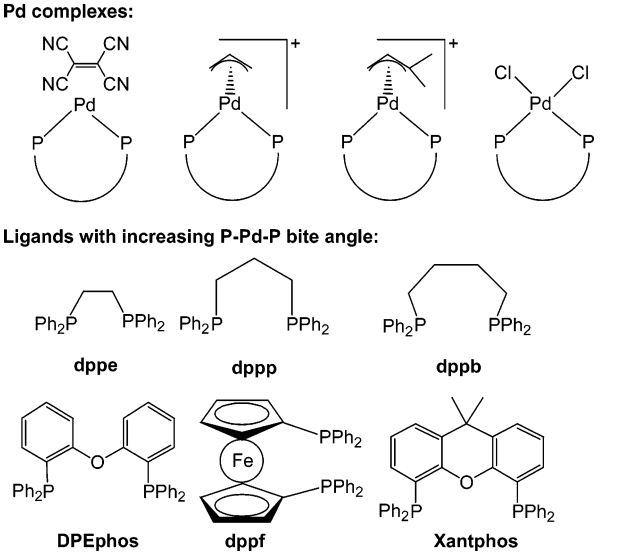

Here, a series of (PP)Pd(XX) complexes are characterized with Pd K-edge XANES spectroscopy, in which the 1s to 5p orbital transition is primarily probed. This provides information about empty molecular orbitals that consist of, or hybridize (mix) with, the metal Pd 5p orbital. We will show that this technique is very suitable for probing the molecular orbitals of the Pd organometallic complexes and gives detailed information about the covalent binding and charge redistribution within these systems. Additional ab initio full multiple scattering calculations with the FEFF8 code have been performed to validate the electronic structure of these Pd complexes. This study demonstrates that XANES spectroscopy is a very powerful tool in unraveling the electronic properties of these organometallic complexes and leads therefore to a better understanding of their properties such as catalytic activity and selectivity. Different coordination moieties (XX) are used to determine oxidation state trends and different (PP) ligands with different bite angles are used to determine bite angle trends. Scheme 1 provides an overview of the different complexes under investigation.

The coordinating moieties (XX) are tetracyanoethylene (TCNE), allyl $[(C_3H_5)]^-$, 1,1-dimethyl-allyl $[(1,1\text{-}(CH_3)_2\text{-}C_3H_3)]^-$, and chloride (2 Cl^-), respectively. The oxidation state of Pd in these complexes is increasing for these moieties from a formal Pd oxidation state of 0 for the neutral (PP)Pd(TCNE) complexes to a formal Pd oxidation state of 2+ for the neutral (PP)Pd(II) complexes with two ionicly bonded Cl^- ions. The (PP)Pd(allyl/dimethyl-allyl) complexes are cationic (PP)Pd(II) complexes with a (mainly) covalently bonded allyl anion moiety. The effective Pd oxidation state will consequently go down from the formally 2+ toward 1+.[12] In this study, the "formal" oxidation state of both the $[(PP)Pd(allyl)]^+$ and $[(PP)Pd(1,1\text{-dimethylallyl})]^+$ complexes will be taken as 1+ to clearly distinguish between the different series. The Pd oxidation states, determined with XANES spectroscopy, will be further addressed as the effective Pd oxidation state. No quantification of the oxidation states will be done and only the trends are considered.

(8) Tromp, M.; van Bokhoven, J. A.; van Haaren, R. J.; van Strijdonck, G. P. F.; van der Eerden, A. M. J.; van Leeuwen, P. W. N. M.; Koningsberger, D. C. *J. Am. Chem. Soc.* **2002**, *124*(50), 14814.
(9) For example, (a) Szabó, K. J. *Organometallics* **1996**, *15*, 1128 and references therein. (b) Aranyos, A.; Szabó, K. J.; Castaño, A. M.; Bäckvall, J.-E. *Organometallics* **1997**, *16*, 1058. (c) Delbecq, F.; Lapouge, C. *Organometallics* **2000**, *19*, 2716.
(10) Koningsberger, D. C.; Mojet, B. L.; van Dorssen, G. E.; Ramaker, D. E. *Top Catal.* **2000**, *10*, 143−155.
(11) For example, Cu XANES: (a) DeBeer, S.; Randall, D. W.; Nersissian, A. M.; Selverstone Valentine, J.; Hedman, B.; Hodgson, K. O.; Solomon, E. I. *J. Phys. Chem. B* **2000**, *104*(46), 10814. (b) DuBois, J. L.; Mukherjee, P.; Stack, T. D. P.; Hedmann, B.; Solomon, E. I.; Hodgson, K. O. *J. Am. Chem. Soc.* **2000**, *122*, 5775. (c) Kau, L.-S.; Spira-Solomon, J.; Penner-Hahn, J. E.; Hodgson, K. O.; Solomon, E. I. *J. Am. Chem. Soc.* **1987**, *109*, 6433. V XANES: (d) Frank, P.; Hodgson, K. O. *Inorg. Chem.* **2000**, *39*, 6018. (e) Wong, J.; Lytle, F. W.; Messmer, R. P.; Maylotte, D. H. *Phys. Rev. B.* **1984**, *3*, 5596. Fe XANES: (f) Westre, W. E.; Kennepohl, P.; DeWitt, J. G.; Hedman, B.; Hodgson, K. O.; Solomon, E. I. *J. Am. Chem. Soc.* **1997**, *119*, 6297.
(12) van Haaren, R. J. Ph.D. Thesis, University of Amsterdam, Amsterdam, The Netherlands, 2002.

A series of bidentate diphosphine ligands are used which induce increasing P−Pd−P bite angles (Scheme 1), that is, dppe 1,2-bis(diphenylphosphino)ethane, dppp 1,2-bis(diphenylphosphino)propane, dppb 1,2-bis(diphenylphosphino)butane, dppf 1,2-bis(diphenylphosphino)ferrocene, DPEphos 2,2-bis(diphenylphosphino(diphenyl ether), and Xantphos. The corresponding bite angles as determined from crystal structure analyses are summarized in Table 1.[4,7a,13,14]

Methods

Experimental. Synthesis of (PP)Pd(XX) Complexes. The (PP)Pd(TCNE),[13] $[(PP)Pd(allyl)]^+$ complexes[7b,15,16] with counterion $[OTf^-]$ or $[BF_4^-]$ and $(PP)PdCl_2$ complexes[14,17,18] were synthesized as described in the literature.

EXAFS Data Collection. Palladium K-edge (24350.0 eV) EXAFS spectra were measured at the European Synchrotron Radiation Facility (ESRF) in Grenoble, France, Beamline 29, and at the Hamburger Synchrotronstrahlungslabor (Hasylab), Germany, Beamline X1. At both beamlines, a Si(311) double crystal monochromator was used. The monochromators were detuned to 50% intensity to avoid effects of higher harmonics present in the X-ray beam. The measurements were performed in the transmission mode using optimized ion chambers as detectors. To decrease noise, three scans were averaged for each sample. A Pd foil is simultaneously measured with each sample. The spectra are energy calibrated by aligning the first peak of the first derivative of the Pd foil to 24350.0 eV.

Negative Second Derivatives XANES Data. To highlight different features present in the Pd K-edge more clearly, the negative second derivative of the normalized absorption data is taken by using the Savitsky−Golay smoothing and differentiation procedure. The first[11d,e] and negative second derivative procedure[11a,b,f] has been used previously by Hodgson et al. and others.[11] In this work, the negative second derivative is calculated on an energy grid of 250 points separated by 0.5 eV, using a smoothing order of 7, which is the number of surrounding points to be used in computing the smoothed second derivative. This results in a second derivative energy window of 3.5 eV.

Theory

Two quite different, but complementary, theoretical calculations are performed on the organometallic complexes to interpret the XANES data and understand and validate the results obtained. Density functional theory calculations (DFT), using the Amsterdam Density Functional (ADF) package,[19] are utilized to calculate the density of states of the allyl and 1,1-dimethylallyl anion moieties. Slater type orbitals are used to represent the atomic orbitals, with basis sets consisting of triple-ζ quality, extended with two polarization functions. These calculations reproduce the bonding orbitals of the system very well. The complete complexes are difficult to calculate and interpret using this method because of the large amount of atoms present and are not discussed here.

These density functional calculations do not approximate the antibonding and continuum orbitals 10−50 eV above the Fermi level adequately because of basis set limitations and because of the use of the ground-state exchange-correlation potential. Therefore, real-space full multiple scattering calculations utilizing a muffin-tin potential are performed on the full Pd complexes. These calculations include a complex-valued exchange-correlation potential (or self-energy) and the effect of the screened core hole and therefore approximate effectively the continuum orbitals, and because of the full multiple scattering, also approximate the strong antibonding resonances present in this energy region.

The FEFF8 code was used to perform ab initio self-consistent field, real-space, full multiple scattering calculations.[20] FEFF8 implements self-consistent field potentials for the determination of the Fermi-level and the charge transfer. The calculations were performed using the Hedin−Lundquist exchange correlation potential. A core hole is included on the absorber atom to mimic the final state of the photon absorption process. The absorption XANES data and the density of states (DOS) are calculated for a relatively narrow bite angle complex $[(dppe)Pd(1,1\text{-}(CH_3)_2{-}C_3H_3)]^+$ ($\beta = 86°$) and two wider bite angle complexes $[(dppf)Pd(1,1\text{-}(CH_3)_2{-}C_3H_3)]^+$ ($\beta = 101°$) and $[(DPEphos)Pd(1,1\text{-}(CH_3)_2{-}C_3H_3)]^+$ ($\beta = 104°$). Neither E_0 nor experimental resolution corrections have been applied.

Results

Pd K-edge XANES data are recorded for the different types of (PP)Pd(XX) complexes and several selected Pd reference complexes, namely, Pd foil, $PdCl_2$, and $PdBr_2$. Figure 1a shows normalized raw XANES data for the Pd references. The Pd K-edge exhibits a very broad edge containing no distinct preedge features, but some small features and shoulders can be observed which vary for the different samples.

To highlight these differences in the Pd K-edge, the negative second derivative of the normalized absorption spectra data, $-d^2\mu/dE^2$, are given in Figure 1b. Clearly, two different peaks can be observed in the spectrum of Pd foil. Moreover, the second feature is split up into two peaks. The spectra of $PdCl_2$ and $PdBr_2$ are dominated by one major peak.

The negative second derivatives of the normalized XANES data for the four different series of palladium complexes (PP)Pd(TCNE), $[(PP)Pd(C_3H_5)]^+$, $[(PP)Pd(1,1\text{-}(CH_3)_2{-}C_3H_3)]^+$, and $(PP)PdCl_2$ are given in Figure 2a−d. The corresponding normalized XANES data are given in the Supporting Information, Figure S1a−d. The negative second derivative accentuates the noise level, and clearly the noise level in the data for the (PP)Pd(TCNE) complexes is somewhat higher than those in the other three series, especially for the (dppf)Pd(TCNE) complex (Figure 2a). With increasing bite angle, some small changes in intensity of the first peak are observed, and the second feature clearly broadens and splits from one peak into two peaks. For the series of $[(PP)Pd(C_3H_5)]^+$ complexes (Figure 2b), larger differences in the intensity of the first peak are observed. Again, the second feature displays a significant broadening and simultaneous splitting upon increasing the bite angle of the ligand. For a larger series of $[(PP)Pd(1,1\text{-}(CH_3)_2{-}C_3H_3)]^+$ complexes (Figure 2c), large deviations in the intensity of the first peak are observed, although no clear trend with bite angle can be easily determined. The second feature again broadens

(13) Kranenburg, M.; Delis, J. G. P.; Kamer, P. C. J.; van Leeuwen, P. W. N. M.; Vrieze, K.; Veldman, N.; Spek, A. L.; Goubitz, K.; Fraanje, J. *J. Chem. Soc., Dalton Trans.* **1997**, 1839.
(14) Hayashi, T.; Konishi, M.; Kobori, Y.; Kumada, M.; Higuchi, T.; Hirotsu, K. *J. Am. Chem. Soc.* **1984**, *106*, 158.
(15) Dent, W. D.; Long, R.; Wilkinson, A. J. *J. Am. Chem. Soc.* **1964**, 1585.
(16) (a) Blöchl, P. E.; Togni, A. *Organometallics* **1996**, *15*, 4125−4132 and references therein. (b) Pretot, R.; Pfaltz, A. *Angew. Chem., Int. Ed.* **1998**, *37*, 323. (c) Vyskocil, S.; Smrcina, M.; Hanus, V.; Polasek, M.; Kocovsky, P. *J. Org. Chem.* **1998**, *63*, 7738.
(17) Steffen, W. L.; Palenik, G. *J. Inorg. Chem.* **1976**, *15*, 2432.
(18) Kranenburg, M.; Kamer, P. C. J.; van Leeuwen, P. W. N. M. *Eur. J. Inorg. Chem.* **1998**, 155.
(19) Amsterdam Density Functional Package ADF 2000.02, Department of Theoretical Chemistry, Vrije Universiteit, Amsterdam; http://www.scm.com.
(20) Ankudinov, A. L.; Ravel, B.; Rehr, J. J.; Conradson, S. D. *Phys. Rev. B.* **1998**, *58*, 7565.

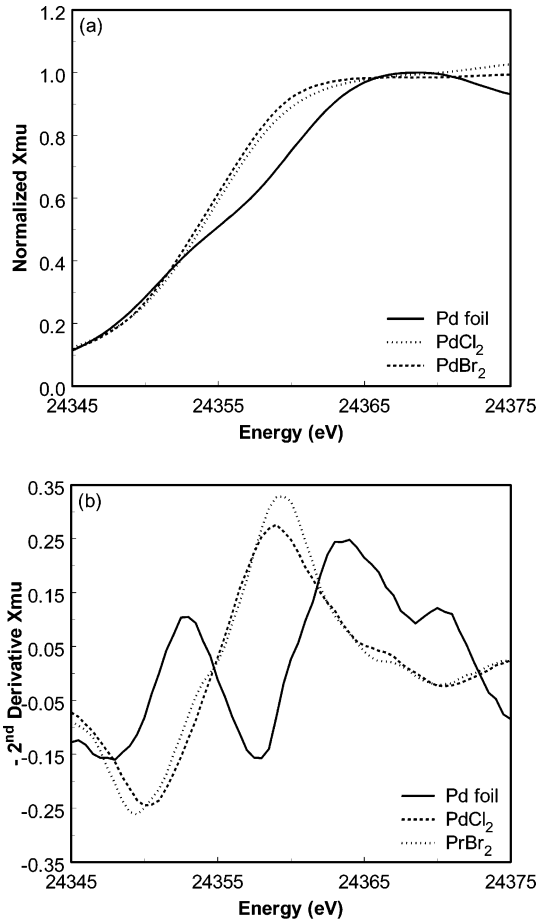

Figure 1. Pd K-edge X-ray absorption data of Pd references (a) normalized XANES spectra, (b) negative second derivative of the normalized XANES data.

and splits with increasing bite angle. For the (PP)$PdCl_2$ series (Figure 2d), only small changes in the first peak and a small shift in the second feature of the negative second derivative are observed when changing the ligand.

Discussion

Dependence of XANES on Pd Symmetry. The negative second derivative spectrum of a palladium foil exhibits two clear features, whereas in those of the $PdCl_2$ and $PdBr_2$ references only one peak is observed (Figure 1b). The crystal structure of Pd foil is face-centered cubic (fcc) with each Pd having 12 nearest neighbors. In this symmetry, the Pd p orbitals hybridize with the Pd d and s orbitals. The Pd K-edge probes the 1s to 5p orbital transition. The 1s to 4d transition is formally dipole forbidden, though a small intensity may originate from the quadruple transition.[11] Loss of the centrosymmetric structure around the Pd causes hybridization of the Pd p with the Pd d orbitals, enabling the dipolar transition to occur at the energy of the quadrupolar transition, that is, the first peak in the negative second derivative. Because of the dominant Pd d character, we will call this the Pd d peak. The second peak originates from the allowed 1s to 5p orbital transition and is further denoted as the Pd p peak. We consider this peak the absorption edge. Because of the symmetry around the Pd atom in the foil, the Pd p density of states (DOS) is split as shown by the second feature in this Pd p peak.

The $PdCl_2$ and $PdBr_2$ solids have square planar D_{4h} symmetry with each Pd surrounded by four Cl^- or Br^- ions. (The orbital diagram for D_{4h} symmetry is shown in the Supporting Information, Figure S2.) The symmetries of the Pd d orbitals compared to the Pd p orbitals are different in square planar geometry; therefore, mixing of these orbitals is not allowed and only one peak, the Pd p peak, is observed in the negative second derivative of the XANES data. Thus, the presence of a Pd d peak, as observed for all (PP)Pd(XX) complexes in this study, indicates a lowering of the square planar geometry.

Dependence of XANES on the Formal Pd Oxidation State. The position of the Pd p peak in the negative second derivative of the XANES data of the $PdCl_2$ and $PdBr_2$ is shifted downward in energy by almost 5 eV relative to Pd foil. This shift reflects the increasing effective oxidation state of the complexes going from a formal oxidation state of 0 for Pd foil to a formal valence state of 2+ for $PdCl_2$ and $PdBr_2$.

The energy $h\nu$ of the metal X-ray absorption edge is determined by the difference between the energy of the initial state, that is, the core level at energy E_C from which the electron is ejected, and the final state, that is, the valence level at energy $E_V + U_{CV}$ that accepts the electron in the final state as illustrated in Figure 3. Here, U_{CV} is the core hole electron attraction energy, which the final valence electron experiences because of the presence of the core hole.

With increasing oxidation state of the metal atom, the orbitals generally contract thereby lowering the energy of the initial state (solid line in Figure 3). This is the usual shift observed in similar core-level X-ray photoelectron spectroscopy (XPS) data.[21] The final state can respond in different ways depending on the nature and localization of the valence state. The increased Coulomb charge with increasing metal oxidation state is mainly felt by electrons on the metal. Consequently, the energy of the metal valence orbitals is large and the energy of the final state will shift similar to the energy of the core level E_C (dashed line (M) in Figure 3). Because the U_{CV} also increases with oxidation state, the shift of $E_v + U_{cv}$ may be even larger than that for E_C. As a result, the energy difference between the initial and final state is decreasing as observed in the energy of the absorption edge. This is what we observe for the Pd complexes, since the energy of the absorption edge decreases with increasing the Pd oxidation state (Figure 1).

More often, the K-edge increases with metal oxidation state.[11] This occurs when the final state is localized on the ligand. In such a case, the final state does not experience the full increased Coulomb potential from the core hole on the metal atom; thus, the final state remains relatively unshifted (dashed line (L)) as shown in Figure 3. The decreasing photon energy with oxidation level in the Pd complexes reported in this study indicates that the charge density in the final Pd p state is mainly localized at the metal absorber atom.

In these organometallic Pd complexes, the formal Pd oxidation state is increasing for the series (PP)Pd(TCNE), $[(PP)Pd(C_3H_5)]^+$, $[(PP)Pd(1,1\text{-}(CH_3)_2{-}C_3H_3)]^+$, and (PP)$PdCl_2$. The position of the absorption edge (Pd p peak) is determined by calculating the centroid of this peak or, in case of splitting, the centroid of the two overlapping peaks. The energy position of the centroid is plotted in Figure 4 as a function of the "formal" oxidation state of the Pd atom. The formal Pd oxidation states of the $[(PP)Pd(allyl)]^+$ and $[(PP)Pd(1,1\text{-dimethyl-allyl})]^+$ are

(21) *Handbook of X-ray Photoelectron Spectroscopy*; Moulder, J. F., Stickle, W. F., Sobol, P. E., Bomben, K. D., Eds.; Physical Electronics, Inc.: Eden Prairie, MN, 1995.

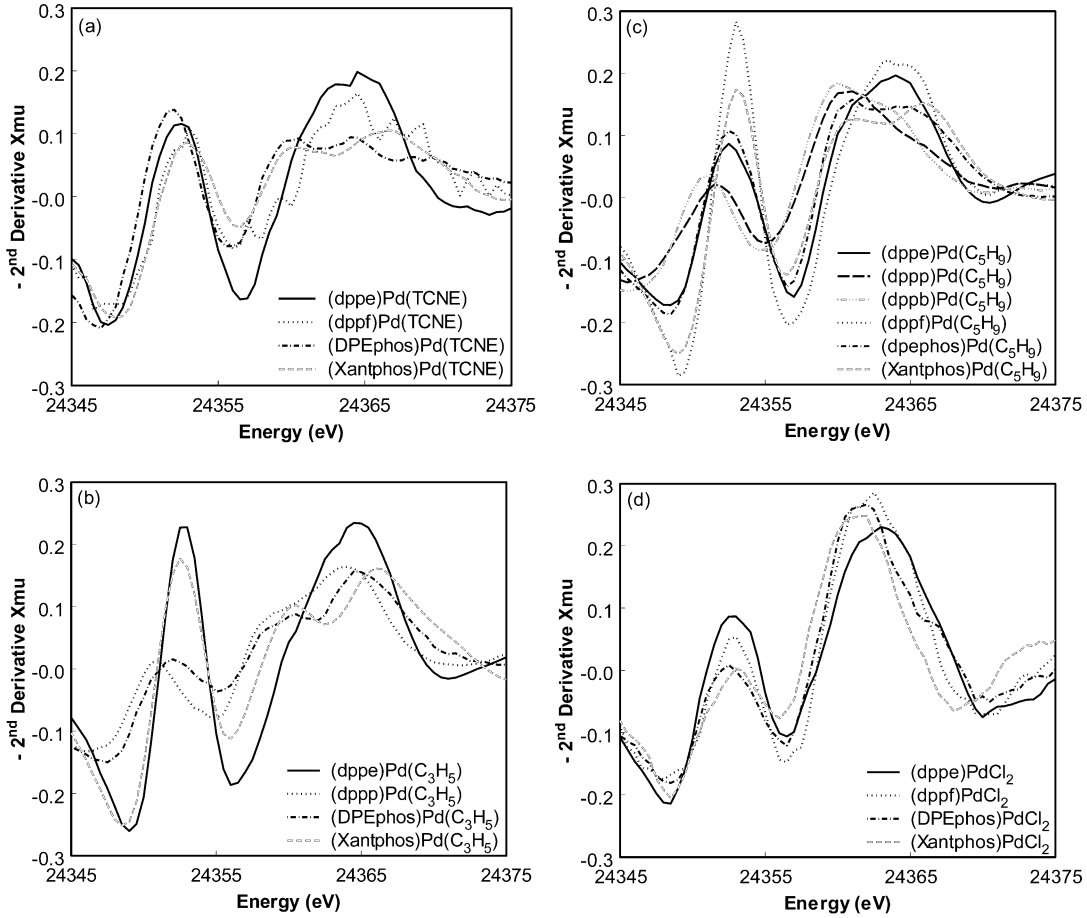

Figure 2. Negative second derivative of Pd K-edge XANES data of series of bidentate diphosphine ligand palladium complexes (PP)Pd(XX), with a series of bite angles. (a) (PP)Pd(TCNE), (b) (PP)Pd(C_3H_5), (c) (PP)Pd(C_5H_9), (d) (PP)$PdCl_2$.

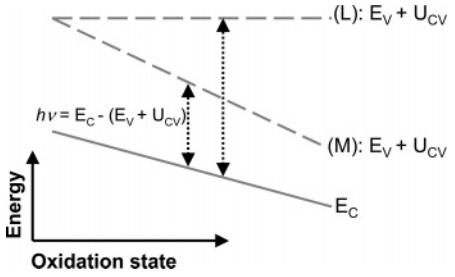

Figure 3. Energy of the metal K-edge X-ray absorption edge as a function of metal oxidation state. The energy $h\nu$ is determined by the energy of the initial state (E_C = core level energy) and final state (E_V = valence level energy). (L) Final state mainly located on the ligand; (M) final state mainly localized on the metal (absorber).

taken as 1+ in this figure to clearly distinguish between the different series. It is observed in this figure that for a certain (PP) ligand the energy of the centroid is decreasing with increasing oxidation state of the Pd, as expected. Figure 4 also shows that within a series of coordinating moiety (XX), the effective oxidation state also depends on the bite angle, which will be further discussed below.

Dependence of the MO Structure on Bite Angle. To be able to understand and interpret the different changes observed in the Pd d and Pd p peaks, the different molecular orbital interaction diagrams of the (PP)Pd(XX) complexes studied have to be established first.

By changing the backbone of a bidentate diphosphine ligand, the P−Pd−P bite angle can be changed systematically (Table 1). This change in geometry will have a steric influence on the metal complex but it will also induce an electronic effect.[12] The effect of the bite angle on the energy of the molecular orbitals and the charge redistribution in the (PP)Pd complexes can be understood by investigating the ligand−metal (LL)M orbital interaction diagram, the so-called Walsh diagram[4,22,23] given in Figure 5.

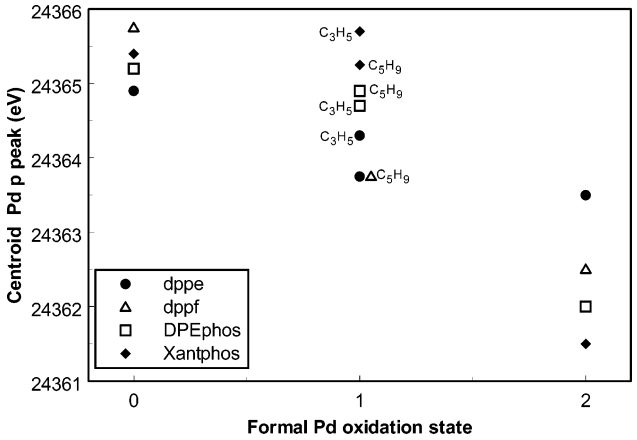

Figure 4. The position of the Pd p peak in the second derivative of the XANES data, determined by the centroid of the total peak, as a function of "formal" Pd oxidation state, that is, coordinating moiety (XX) for series of bidentate diphosphine palladium complexes (PP)Pd(XX).

(22) Yoshida, T.; Tatsumi, K.; Otsuka, S. *Pure Appl. Chem.* **1980**, *52*, 713.
(23) Otsuka, S. *J. Organomet. Chem.* **1980**, *200*, 191.

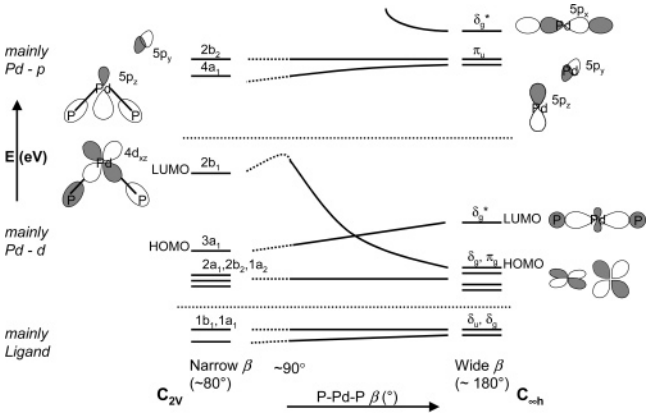

Figure 5. Walsh diagram for Pd(PP) complexes.

Table 2. Group Symmetry Matrices for (a) C_{2v} and (b) C_s Symmetry

(a)

C_{2v}	E	C_2	$\sigma_v(xz)$	$\sigma_v'(yz)$		
A_1	1	1	1	1	z	x^2, y^2, z^2
A_2	1	1	−1	−1	R_z	xy
B_1	1	−1	1	−1	x, R_y	xz
B_2	1	−1	−1	1	y, R_x	yz

(b)

C_S	E	σ_h		
A′	1	1	z, y	x^2, y^2, z^2, yz
A″	1	−1	x	xy, xz

The Walsh diagram was calculated for d^{10}-metal complexes and a bite angle range of 90−180° (solid lines in Figure 5). The diagram is based on the extended Hückel MO method, assuming C_{2v} symmetry for the L−M−L complex (Table 2a), and only σ-type orbitals for the ligands are considered.[22,23] Only the relevant ligand metal interactions (metal 4d and 5p orbitals) are shown in Figure 5. The lower two orbitals originate primarily from the ligand, in our case the P donor atoms. At higher energy, the five Pd 4d and the three Pd 5p orbitals are shown. The antibonding δ_g* or $3a_1$ orbital is constructed from an out-of-phase combination of mainly Pd $4d_{z2}$ and L 3s atomic orbitals and stabilizes with decreasing bite angle. As the L−M−L bite angle decreases (bending in the *xz* plane), the L 3s orbitals start to mix in with the $5p_x$ and $4d_{xz}$ of the metal, resulting in the formation of the hybridized orbital $2b_1$. With decreasing bite angle, the $5p_x$ component of this orbital decreases, while the $4d_{xz}$ character increases.

The $[(PP)Pd]^{2+}$ fragment of the complexes in this work are considered to have a d^8 metal electron configuration regardless of oxidation state, that is, the first four Pd 4d orbitals are occupied (Figure 5). For a complex with a relatively narrow bite angle of 90°, the $2b_1$ molecular orbital is the lowest unoccupied molecular orbital (LUMO), whereas for linear complexes with a P−Pd−P angle of 180°, the δ_g* orbital is the LUMO. The character of the HOMO and LUMO orbitals thus switch with the bite angle increasing from 90° to 180°. Since Pd complexes in the bite angle range 80−110° are studied in this work, the Walsh diagram is extrapolated to bite angles smaller than 90° (dotted lines in Figure 5). This extrapolation is based on the experimental results and theoretical considerations presented here (vide infra). In summary, the Walsh diagram shows that changing the bite angle of the complex

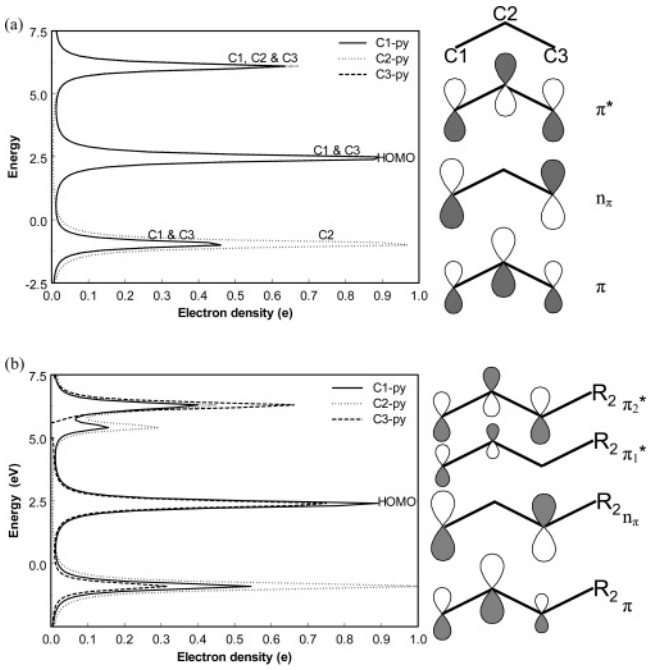

Figure 6. Calculated density of states and corresponding (quantitative) orbital pictures of (a) plain allyl C_3H_5 and (b) 1,1-disubstituted allyl C_5H_9.

results in large changes in both the position and symmetry of the Pd 4d and Pd 5p orbitals.

Dependence of the MO Structure on Allyl Interaction. The Walsh diagram (Figure 5) ignores the interaction of the $[(PP)Pd]^{2+}$ fragment with the coordinating moiety (XX). For a more complete description of the (PP)Pd(XX) complexes, these interactions must also be included, especially in cases where this interaction is covalent in nature. In the $(PP)PdCl_2$ complexes, the Pd has a formal oxidation state of 2+. The electronegative chloride ion forms an almost pure ionic bond with palladium. The Cl^- atomic orbitals therefore have large binding energies and undergo little interaction with the Pd atom orbitals. Consequently, the orbital interaction diagram for this series of complexes is similar to the Walsh diagram shown in Figure 5.

On the other hand, the allyl moieties interact mainly covalently to the $[(PP)Pd]^{2+}$ ligand fragment. The orbital interaction diagram between $[(PP)Pd]^{2+}$ and a $(C_3H_5)^-$ moiety has already been described and discussed in the literature.[9] The $[(PP)Pd(C_3H_5)]^+$ complex has a lower symmetry C_S relative to the C_{2v} symmetry of the $[(PP)Pd]^{2+}$ fragment (Table 2b). Since the complexes studied in this work have bite angles of 80−110°, the molecular orbital levels calculated for narrow bite angles (Figure 5) are used to construct the orbital interaction diagram between the $[(PP)Pd]^{2+}$ fragment and the coordinating allyl moiety.

Two π orbitals (bonding and antibonding) and one nonbonding π orbital (n_π) are present within the allylic fragment. The density of states (DOS), calculated using density functional theory as incorporated into the ADF code, and consequent orbital pictures are shown in Figure 6a and agree with literature results.[9,12] The relative sizes of the p orbitals on each C atom indicate their relative contributions obtained from the ADF calculations. Coordination of the allyl moiety to the $[(PP)Pd]^{2+}$ fragment causes the $2b_1$ (LUMO) (PP)Pd $4d_{xz}$ orbital (taken from the Walsh diagram Figure 5) to interact with the n_π orbital

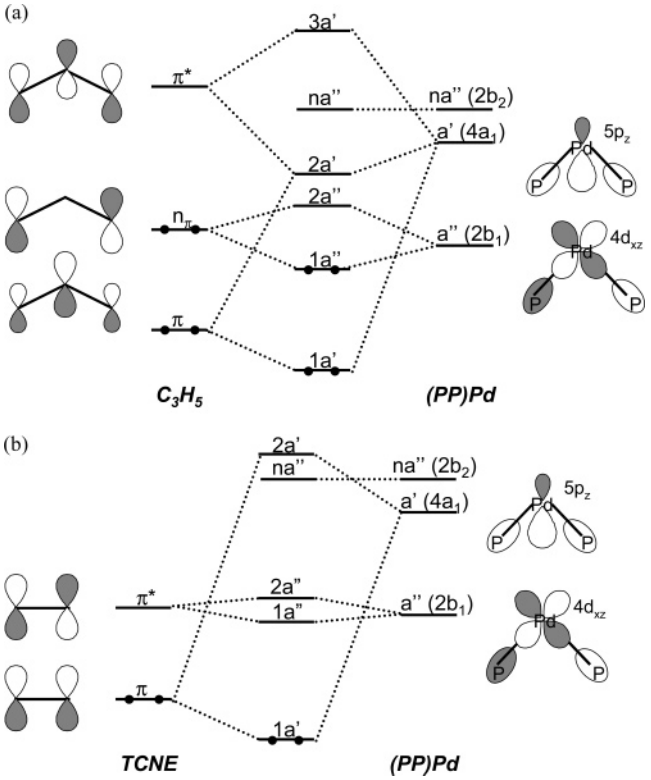

Figure 7. Orbital interaction diagram for (a) (η_3-allyl)Pd(P−P) and (b) (TCNE)Pd(PP) complexes.

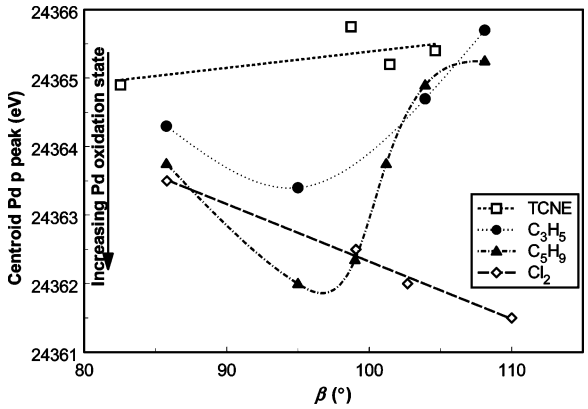

Figure 8. The position of the Pd p peak in the negative second derivative of the XANES data, determined as the centroid of the total feature, as a function of bite angle for all series of bidentate diphosphine palladium complexes (PP)Pd(XX).

forming orbitals 1a″ (filled) and 2a″ (nonfilled) as shown in Figure 7a. Since after coordination of the allyl to the [(PP)-Pd]$^{2+}$ fragment, the symmetry of the complex is lowered from C_{2v} to C_S, the orbital $2b_1$ should now be denoted as a″ (see Figure 7a and Table 2). The bonding π and antibonding π^* orbitals of the allylic fragment interact with the (PP)Pd-5p_z $4a_1$ or a′ orbital, as can be expected from the symmetry of the three orbitals (Figures 5, 6a, and 7a), and form one filled and two nonfilled MOs, 1a′, 2a′, and 3a′. The (PP)Pd-5p_y $2b_2$ orbital is close in energy too, but this orbital is not able to interact with the allyl moiety as it lies perpendicular to the plane of the complex (see Figures 5 and 6a). In Figure 7a, this $2b_2$ orbital ends up in the orbital interaction diagram as a nonbonding orbital. The Pd 5p_x orbital is able to mix with the 4d_{xz} orbital as both are of b_1 symmetry in the C_S point group, but the extent

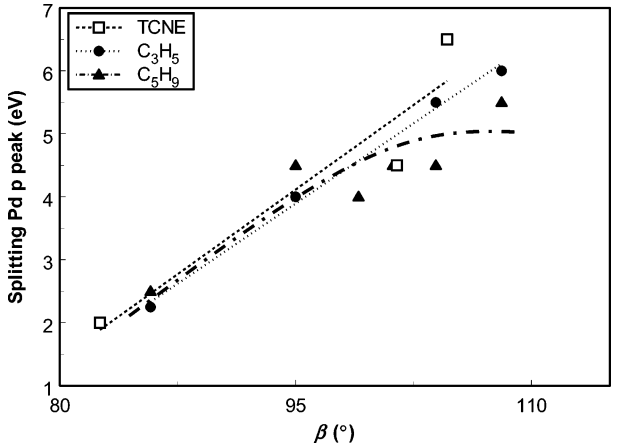

Figure 9. The splitting of the Pd p peak in the second derivative of the XANES data as a function of bite angle, for series of bidentate diphosphine ligand palladium complexes (PP)Pd(XX).

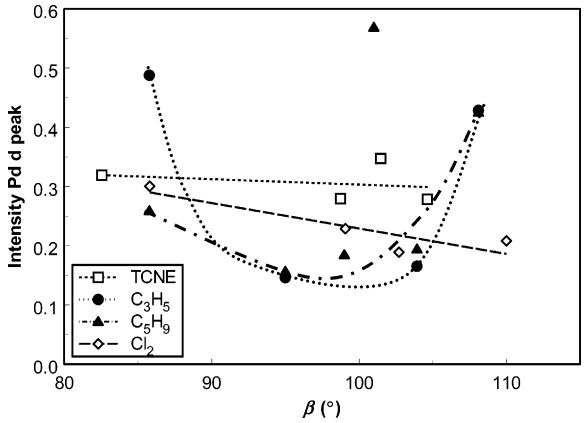

Figure 10. The intensity of the Pd d peak observed in the second derivative of the XANES data as a function of bite angle, for all series of bidentate diphosphine ligand palladium complexes (PP)Pd(XX).

of this mixing depends strongly on the symmetry and bite angle of the complex.

The assignment of either 2a′ or 2a″ as the LUMO has been discussed in the literature.[9] It was suggested that for π-acceptor ligands such as phosphine, the Pd d orbitals (a″) are destabilized because of back-donation of charge from the metal to the ligand, thereby decreasing the splitting of the 1a″ and 2a″ orbitals. As a result, the 2a″ orbital will be the LUMO. This is exactly what we observe in our XAS data. The 2a″ orbital is mainly Pd d in character whereas the 2a′ consists of mainly Pd p DOS. The Pd d peak stemming from the 2a″ orbital is always the lowest energy (first) peak for the complexes studied here and is thus the LUMO in these complexes.

The Pd d peak is visible in the XANES, which reflects only p DOS, because of some hybridization of the Pd 4d_{xz} with the Pd 5p_x orbital in these low symmetry complexes. The Pd d peak was not observed in the square-planar reference samples as discussed above. Although the Pd d orbital energy is sensitive to changes in the bite angle as indicated in Figure 5, the 2a″ (Pd 4d_{xz}) orbital remains the first peak regardless of bite angle (<110° for the complexes studied). The presence of a Pd d peak for all the complexes studied indicates that the LUMO is indeed the $2b_1$ orbital throughout the 80−110° bite angle range. This is expected, since the $3a_1$ orbital cannot overlap with the nonbonding allylic orbital n_π because of its b_1 symmetry (Figures 5 and 7a). Thus, the left part of the Walsh diagram shown in

Figure 5 is valid for the $[(PP)Pd(allyl)]^+$ complexes discussed in this work and the LUMO/HOMO orbital switch is believed to occur at bite angles larger than 110°.

The orbital interaction diagram in Figure 7a also explains the observed splitting of the Pd p peak in the negative second derivative of the XAS data. Overlap of the empty (PP)Pd-5p_z orbital with the allyl moiety π* orbital results in a bonding (2a′) and antibonding (3a′) molecular orbital combination. Additionally, the nonbonding Pd-5p_y ($2b_2$) peak, na″, is present between 2a′and 3a′. The Pd K-edge XANES probes the lower-energy 2a′ and na″ molecular orbitals. The 3a″ molecular orbital is not detected since it is probably too high in energy and consequently severely broadened with the continuum orbitals.

The 1,1-dimethyl-substituted allyl $[(PP)Pd(1,1\text{-}(CH_3)_2{-}C_3H_3)]^+$ complexes possess a similar orbital interaction diagram as the unsubstituted allyl (Figure 7), but the symmetry of the allyl orbitals is different. The density of states of the $(1,1\text{-}(CH_3)_2{-}C_3H_3)$ anion calculated with ADF is presented in Figure 6b. The shapes and sizes of the molecular orbitals indicate that the allylic orbitals of $(1,1\text{-}(CH_3)_2{-}C_3H_3)^-$ are slightly asymmetric, with the unsubstituted carbon atom (C_1) more pronounced in the bonding π molecular orbital and the substituted carbon atom (C_3) more pronounced in the antibonding π_2* molecular orbital. An additional antibonding π_1* molecular orbital is formed; its size, however, is very small and its symmetry does not allow overlap with the $[Pd(PP)]^{2+}$ fragment. From modeling and single-crystal X-ray analysis studies, it is known that with increasing bite angle, steric hindrance causes the allyl coordination to shift from an η_3-allyl to a more η_1-η_2-like coordination.[7a−b,12,24]

The coordination of the TCNE molecule to the $[(PP)Pd]^{2+}$ fragment is, like the allyl moieties, covalent in character. Because of the simpler alkene molecular orbital structure, pure π bonding and π* antibonding overlap occurs with the Pd. The orbital interaction diagram simplifies to that shown in Figure 7b. The π orbital interacts with the Pd p orbital and the Pd d orbital interacts with the allyl π* orbital. The Pd d bonding and antibonding molecular orbitals (1a″ and 2a″) are now probably both present in the feature appearing near the threshold in the XANES data and may account for the broadening of this feature compared to the Pd d peaks in the other complexes. The broadening and splitting of the higher energy Pd p feature is slightly different compared to the allyl complexes; it now arises from the separation between the nonbonding (na″) and antibonding (2a′) orbital, the latter now lower in energy compared with the 3a′ in the allyl case.

Changes in the XANES with Bite Angle. The negative second derivatives of the XANES data (Figure 2a−d) show multiple differences with varying the bite angle of the complexes. The reason for these changes can now be explained in terms of the molecular orbital interaction diagrams discussed above.

We first consider the changes in the Pd p peak since these are more pronounced than those for the Pd d peak. Except for the (PP)$PdCl_2$ series, a splitting of the Pd p peak is observed with increasing bite angle. Moreover, the position of the Pd p peak shifts with bite angle and as expected with oxidation state (Figure 4). To study these changes in more detail, three different

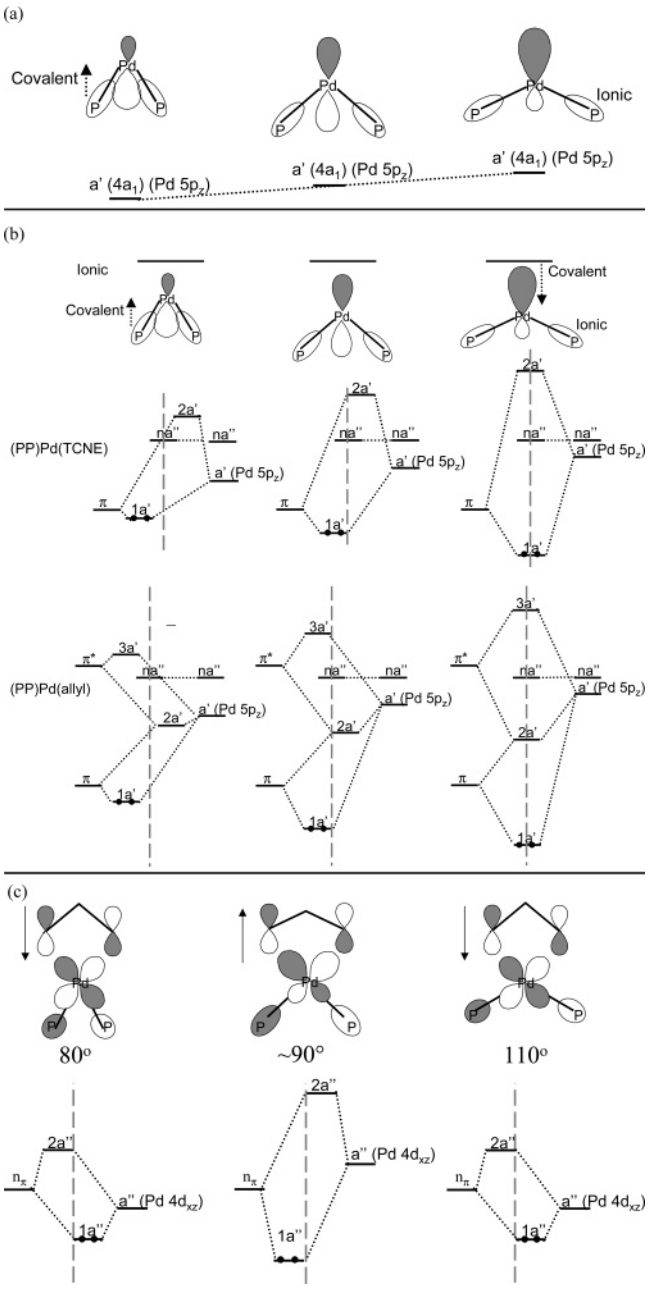

Figure 11. Orbitals in (PP)Pd(XX) complexes and charge distribution with increasing bite angle (a) within (PP)Pd fragment and with coordinating moiety via (b) Pd 5p_z orbitals for complexes with covalent bonded moieties (TCNE and allyl moieties indicated by horizontal line) and (c) Pd 4d_{xz} orbitals for allyl complexes. The placement of MO orbital lines about vertical center lines (gray striped lines) reflect relative atomic charge distribution in MO, but the relative positions are exaggerated for clarity. Vertical arrows indicate direction of charge redistribution.

plots are constructed as a function of the bite angle within the different series (Figures 8−10). The energy centroid of the Pd p peak is plotted in Figure 8 and the splitting of the Pd p peak defined as the energy difference between the two component features is plotted in Figure 9. The intensity of the Pd d peak versus bite angle is plotted in Figure 10. Each of these figures is discussed in separate sections below.

Pd p Centroid Energy: An Indicator of the Oxidation State of Pd. The Pd oxidation states, determined with XANES spectroscopy, are clearly changing with coordinating moiety (XX) and bite angle ((PP) ligand). These measured Pd oxidation

(24) Åkermark, B.; Zetterberg, K.; Hansson, S.; Krakenberger, B.; Vitagliano, A. *J. Organomet. Chem.* **1987**, *335*, 133.

states will be further addressed as the effective Pd oxidation states. No further quantification of the oxidation states will be done and only the trends are considered here.

Figure 4 showed that the energy of the Pd p peak decreases with increasing the formal oxidation state from 0 in Pd foil to 2+ in $PdCl_2$ and $PdBr_2$. This shift can therefore serve as an indicator of the Pd oxidation state. The position of the Pd p peak as a function of the bite angle is displayed in Figure 8 for the different (PP)Pd(XX) series. Linear correlations are found for the (PP)$PdCl_2$ and (PP)Pd(TCNE) series. The slopes of these correlations, however, differ significantly in size and sign. The (PP)Pd(TCNE) series shows a small decrease in effective oxidation state with increasing bite angle, whereas the (PP)-$PdCl_2$ complexes show a larger increase in effective oxidation state with bite angle. The allyl series, both $[(PP)Pd(C_3H_5)]^+$ and $[(PP)Pd(1,1\text{-}(CH_3)_2{-}C_3H_3)]^+$ complexes, show a minimum in energy position, that is, a maximum in effective oxidation state at intermediate bite angles. The effective oxidation state of the $[(PP)Pd(C_3H_5)]^+$ complexes is always lower than for the analogous $[(PP)Pd(1,1\text{-}(1,1\text{-}(CH_3)_2{-}C_3H_3)]^+$ complexes.

The change in effective Pd oxidation state of the (PP)$PdCl_2$ complexes with bite angle are dominated by a charge redistribution within the metal−ligand system, since the metal−Cl bond is mainly ionic and is thus not expected to be dependent on the bite angle. The (PP) ligand 3s overlaps with the Pd $5p_z$ orbital forming the $4a_1$ molecular orbital (Figure 5). This overlap decreases with increasing P−Pd−P bite angle, as shown schematically in Figure 11a. This results in a more ionic Pd − (PP) bond. As a consequence, the (PP) ligand cannot effectively donate electron density to the Pd center, resulting in an increased oxidation state of the Pd atom with increasing bite angle. Since all studied Pd complexes have similar (PP) ligands, this reduced electron density donation of the PP ligands in the $4a_1$ (or a′) molecular orbital with increasing bite angle occurs in all the (PP)Pd(XX) complex series regardless of the (XX) moiety. For the (PP)$PdCl_2$, this is the only charge redistribution effect.

The TCNE complexes also display a linear behavior of oxidation state with bite angle, however, with the opposite trend as the dichloride complexes. In contrast to the ionic Pd−Cl bonds, the coordinating TCNE moiety is (mainly) covalently bonded to the Pd atom, that is, the Pd p and Pd d orbitals are covalently overlapping with the coordinating TCNE orbitals to form the a″ and a′ molecular orbitals. As shown in Figure 7b, only the 1a′ molecular orbital is occupied and can donate electron density to the Pd. Figure 11b illustrates that while the Pd−(PP) ligand overlap decreases (as was shown in Figure 11a), the Pd−TCNE overlap increases for complexes with wider bite angles. It is this change in the 1a′ molecular orbital which results in donation of electron density from the TCNE moiety to the Pd thereby decreasing the effective Pd oxidation level, that is, charge-back-donation is dominating here.

For the two series of allyl and 1,1-disubstituted allyl (PP)Pd complexes, a maximum in the effective Pd oxidation state is observed at a bite angle of around 95−100°. Moreover, the total maximum variation in oxidation states is larger than that of the (PP)$PdCl_2$ or (PP)Pd(TCNE) complexes. These observations strongly suggest that additional charge redistribution involving the Pd d orbitals is occurring in these systems. Figure 11c illustrates why this occurs. The Walsh diagram in Figure 5 already shows that the $2b_1$ LUMO decreases sharply in energy as the bite angle increases above 90°. From Figure 11c it is clear that this originates from antibonding overlap with orbitals from the PP ligands, with a maximum at a bite angle ∼90°. This change in antibonding character changes the energy of the Pd $4d_{xz}$ orbital. Because of the shape of the Pd $4d_{xz}$ orbital, the strongest Pd (PP) ligand antibonding overlap will occur at ∼90°, where it has a maximum in energy. The energy shift of the Pd $4d_{xz}$ orbital strongly alters the localization or interaction with the allyl n_π orbital as illustrated. The 1a″ molecular orbital is localized mainly on the allyl for the complex with a bite angle around 90° and shifts to the Pd as the bite angle decreases or increases from 90°. Thus, the charge redistribution for the allylic complexes is dominated by the Pd d orbital, and the maximum Pd oxidation state occurs around 90°.

Although the Pd−allyl charge redistribution is dominated by the Pd d orbitals, charge rearrangement via the a′ molecular orbital, involving the Pd p orbitals, is also occurring as illustrated in Figure 11b. Because of the decreased (PP) ligand−Pd overlap with increasing bite angle, the energy of the Pd $5p_z$ orbital increases and this affects the localization of the 1a′, 2a′, and 3a′ orbitals. At narrow bite angle, the occupied 1a′ molecular orbital is mainly allyl π in character, and with increasing bite angle the overlap with the Pd $5p_z$ orbital increases. This facilitates charge redistribution from the coordination moiety to Pd with increasing bite angle. The increasing covalent interaction with bite angle is similar for both the Pd $5p_z$ with π and Pd $5p_z$ with π^* orbitals and thus also influences the Pd p peak splitting (vide infra).

Although the formal Pd oxidation state for the $[(PP)Pd(C_3H_5)]^+$ and $[(PP)Pd(1,1\text{-}(CH_3)_2{-}C_3H_3)]^+$ complexes is the same, the effective oxidation state of Pd is always lower for the 1,1-di-substituted allyl complexes than for the corresponding unsubstituted allyl complexes. As observed in Figure 6b, the DOS of the n_π orbital on the C_1 and C_3, indicated by the size of the 2p orbital on each carbon atom, is identical in both fragments. This indicates that the charge redistribution via the Pd $4d_{xz}$ orbital, which is overlapping with the n_π orbital, is approximately the same for both series of complexes. For $(1,1\text{-}(CH_3)_2{-}C_3H_3)^-$, however, the π and π^* molecular orbitals show a significant asymmetry between the unsubstituted C_1 and substituted C_3 carbon atoms, that is, larger on the C_1 atom in the π orbital and larger on the C_3 atom in the π^* orbital. This asymmetry makes the electron density redistribution less effective because the Pd $5p_z$ orbital is oriented to maximize the covalent overlap with the π^* orbital. The π^* orbital is closer in energy and therefore the orbital mixing with the occupied π orbital, which is the only orbital through which the charge redistribution is possible, decreases. A net higher effective Pd oxidation state is found for the $[(PP)Pd(1,1\text{-}(CH_3)_2{-}C_3H_3)]^+$ complexes since the allyl π Pd $5p_z$ charge redistribution (via 1 a′) is less effective in this case. At wider bite angles, the Pd oxidation states for the $[(PP)Pd(1,1\text{-}(CH_3)_2{-}C_3H_3)]^+$ complexes may also level off compared to the unsubstituted allyl case because of the distortion of the $(1,1\text{-}(CH_3)_2{-}C_3H_3)^-$ moiety caused by steric hindrance. This is confirmed by the crystal structure showing an increase in $Pd{-}C_{allyl}$ distances and asymmetric bond lengths ($Pd{-}C_1 > Pd{-}C_3$).[24]

The effects of the three different charge rearrangements as described above are shown qualitatively in Figure 12. Depending on the type of overlap between the $[(PP)Pd]^{2+}$ fragment and the coordinating moiety, and the occupation of the molecular

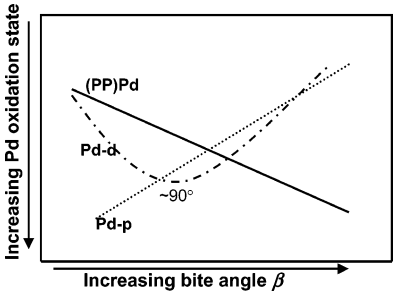

Figure 12. Qualitative effects of the three different charge redistribution mechanisms on the effective Pd oxidation state as a function of bite angle.

Table 3. The Charge Redistribution Effects Occurring within the Different Complexes

	(PP)Pd(TCNE)	(PP)Pd(C_3H_5)	(PP)Pd(1,1-$(CH_3)_2$−C_3H_3)	(PP)$PdCl_2$
(PP)Pd	yes	yes	yes	yes
Pd 5p	yes	yes	yes	no
Pd 4d	no	yes	yes	no

orbitals for the complete (PP)Pd(XX) complex, one, two, or all three charge rearrangements can take place in the complex, as denoted in Table 3.

The change in effective Pd oxidation for the allylic (PP)Pd complexes is large, varying in magnitude from as small as that in the (PP)Pd(TCNE) complexes to as large as that in the (PP)-$PdCl_2$ complexes. This shows the dramatic effect of the bite angle on the oxidation level in these complexes. It should thus not be surprising that this very large change in the oxidation state of the Pd can have enormous effects on the activity and selectivity of these Pd catalytic complexes.[4,7]

Pd p Energy Splitting: An Indicator of the Pd p and Allyl Covalent Interaction. For a large number of the (PP)Pd(XX) complexes, a splitting of the Pd p peak is observed. The magnitude of this splitting is plotted in Figure 9 as a function of the bite angle of the (PP) ligand. The (PP)$PdCl_2$ complexes display only one Pd p peak for the complete bite angle range, that is, no splitting is observed for these complexes and thus no results for the (PP)$PdCl_2$ are displayed in Figure 9.

The presence of only one peak for the (PP)$PdCl_2$ complexes is expected on the basis of the orbital interaction diagram. The $4a_1$ and $2b_2$ molecular orbitals are nearly degenerate when no bonding occurs with the coordinating moiety, visible by the small energy difference in the Walsh diagram in Figure 5, and thus appear as one Pd p peak. The presence of a splitting for the other complexes confirms that it originates from a covalent interaction of Pd with the coordinating allyl and TCNE moieties.

The allyl and TCNE bearing Pd complexes display an increased splitting with increasing bite angle, as shown in Figure 9, which means an increased covalent interaction. The splitting could be determined for only three of the (PP)Pd(TCNE) complexes. Because of the low signal-to-noise ratio of the (dppf)Pd(TCNE) data, a point for this sample could not be determined; thus, the correlation of the linear fit with the points is rather low. A good linear correlation is found between the energy of the splitting and bite angle ($R^2 = 0.99$) for the [(PP)-Pd(C_3H_5)]$^+$ complexes. In contrast, the [(PP)Pd(1,1-$(CH_3)_2$−C_3H_3)]$^+$ complexes show a linear correlation up to a bite angle of about 95−100° after which the curve levels off.

Somewhat surprisingly, the [(PP)Pd(C_3H_5)]$^+$ and [(PP)Pd-(1,1-$(CH_3)_2$−C_3H_3)]$^+$ series display a similar Pd p peak splitting at low bite angles, even though the charge redistribution is less effective for the (1,1-$(CH_3)_2$−C_3H_3) complexes. Apparently, the Pd p−π* covalent interaction is similar for both moieties, regardless of the asymmetry in the (1,1-$(CH_3)_2$−C_3H_3) complexes, as suggested above, and it is only the interaction with the π orbital that severely suffers in the (1,1-$(CH_3)_2$−C_3H_3) case. At wider bite angles, however, the splitting for the (1,1-$(CH_3)_2$−C_3H_3) complexes levels off, whereas the splitting for the unsubstituted allyl (C_3H_5) complexes continues to increase. For large bite angle complexes, the covalent interaction with the (1,1-$(CH_3)_2$−C_3H_3)$^-$ is diminished because of steric hindrance. With increasing bite angle, the symmetry of the (1,1-$(CH_3)_2$−C_3H_3) moiety transforms from a η_3 coordination, identical to C_3H_5, to a distorted n η_1−η_2 like coordination[7a−b,12,24] as mentioned before.

The (PP)Pd(TCNE) series shows the largest splitting, that is, largest covalent interaction, consistent with the larger radial extent of the Pd d orbitals in a Pd complex with a formal oxidation state of zero. Its increased slope at larger bite angle is also consistent with this.

Pd d Intensity: An Indicator of Charge Redistribution Involving the Pd d Orbitals. The first peak in the negative second derivative of the normalized XAS data, the Pd d peak, shows clear changes in intensity for the different complexes. The intensity of this peak, determined by taking the difference in magnitude between the maximum and (left) minimum of this first peak in the negative second derivative, is plotted as a function of bite angle for all complexes (Figure 10). The trends with bite angle show at first glance a striking similarity with the bite angle trends shown in Figure 8 for the Pd p energy centroid. This similarity strongly suggests that the Pd d band intensity is somehow reflecting the Pd oxidation level, at least its change with bite angle. However, the Pd d band intensity is going in the opposite direction from what one initially might expect on the basis of oxidation level, that is, with increasing oxidation one would expect some of the charge removed from the Pd d levels (and this is even seen in Figures 8 and 10 already discussed above). Thus, its intensity is not tracking with the magnitude of the empty Pd d_{xz} DOS in the $2b_1$ molecular orbital but in the opposite direction.

The reason for this reverse correlation can be understood from Figure 11b and the knowledge that the intensity of the Pd d peak does not correlate with Pd d peak intensity in the $2b_1$ molecular orbital but with the amount of mixing in of the Pd $5p_x$ orbital. Since the Pd K-edge XAS is dictated by the dipole approximation for a 1s to 5p transition, the Pd d peak can only be visible after mixing in of the Pd 5p orbital. The Pd $5p_x$ orbital cannot directly mix with the Pd $4d_{xz}$ orbital because they have different symmetry. They do appear together in the $2b_1$ molecular orbital because of a covalent mixing in of either ligand or moiety (XX) orbitals. We already noted in the Walsh diagram of Figure 5 that the (bite angle dependent) mixing of these two components in the $2b_1$ molecular orbital is due to hybridization with the ligand 3s orbital. However, for the small bite angle range of 25° investigated, the change in 3s mixing is expected to be small and in any event monotonic with bite angle, so such mixing involving the ligand cannot explain the observed minima in the Pd d intensity. The mixing in of the allylic n_π orbital, however, enables Pd $5p_x$ to mix in as well. Thus, the intensity of the Pd d peak mainly correlates with the amount of n_π

character in the 2a″ molecular orbital, and this tracks in the reverse direction with the Pd d_{xz} orbital component as illustrated in Figure 11b. Therefore, the intensity of the Pd d peak in the XANES is a measure for the magnitude of the allyl to Pd $4d_{xz}$ orbital charge distribution.

The TCNE and dichloride moieties do not experience any charge redistribution involving the Pd $4d_{xz}$ orbital as indicated above. Even though the Pd $4d_{xz}$ orbitals mix with the TCNE π^* orbital, both the bonding and antibonding 1a″ and 2a″ molecular orbitals are empty, so the Pd d peak is unaffected by this mixing. Nevertheless, the Pd d peak intensity still appears to reflect the Pd oxidation level; thus, it must depend partly on the charge redistribution involving the Pd $5p_z$ orbital. Apparently, the mixing of the Pd $5p_x$ and $4d_{xz}$ orbitals is sensitive to the radial extent of the $5p_x$ orbital; as the oxidation state increases, the contraction of the $5p_x$ orbital decreases this mixing. Thus, through a smaller "second-order" effect, the intensity of the Pd d peak also reflects the oxidation level brought about by charge redistribution facilitated by the Pd p orbitals. For the allylic complexes, the Pd $4d_{xz}$ orbital charge redistribution overrules this second-order effect due to the Pd p orbital screening.

One remark has to be made here. As can be seen for the (1,1-$(CH_3)_2-C_3H_3$) series in Figure 10, the [(dppf)Pd(1,1-$(CH_3)_2-C_3H_3$)]$^+$ complex ($\beta = 101°$) has a very high Pd d peak intensity, which is not consistent with the bite angle trend derived. It is believed that this results from the presence of the Fe atom in the (dppf) ligand. Although the distance of the Fe atom to the Pd atom is ∼4 Å, its radial extent is sufficiently large that it overlaps with the Pd d orbitals and consequently increases the Pd d peak intensity.[25] This is validated with theoretical FEFF8 calculations (see Appendix).

Although the intensity of the Pd d peak appears to mirror the oxidation level with bite angle just like the energy of the Pd p peak does, a more detailed comparison of Figures 8 and 10 reveals significant differences. Further significant differences occur between the (C_3H_5) and (1,1-$(CH_3)_2-C_3H_3$) allyl moieties. These differences include the following:

(a) Whereas Figure 8 shows the oxidation level to be larger for the [(PP)Pd(1,1-$(CH_3)_2-C_3H_3$)]$^+$ complexes, Figure 10 shows the Pd d intensity at the minima to be quite similar. This occurs because the Pd d charge redistribution via the n_π orbital within the Pd−ligand complex is similar in both cases, but the Pd p distribution is much smaller in the (1,1-$(CH_3)_2-C_3H_3$) case because of the asymmetry in the π and π^* orbitals as discussed above.

(b) Whereas Figure 8 shows that the oxidation level reaches a maximum (energy a minimum) around a bite angle of 95° (C_3H_5) to 98° (1,1-$(CH_3)_2-C_3H_3$), the minimum in Pd d peak intensity in Figure 10 occurs around 100° (C_3H_5) to 95° (1,1-$(CH_3)_2-C_3H_3$). Apparently, the Pd d orbital charge redistribution is maximal around 95−100°, and the Pd p orbital charge redistribution is maximal at larger bite angle. When the two effects are added together for the allyl complexes (Figure 8), the maximum oxidation state moves down from 100° to ∼95°. This is confirmed by comparison of the shift in the minima of the two allylic moieties as observed in Figure 10. In the (1,1-$(CH_3)_2-C_3H_3$) case, the Pd p orbital charge redistribution is much less efficient and therefore the two minima, the effective Pd oxidation state and the Pd d peak intensity, occur at approximately the same angle.

(c) The difference in Pd d peak intensity between (PP)Pd(TCNE) and (PP)$PdCl_2$ complexes is small in Figure 10 compared to the much larger difference in Pd p peak position in Figure 8. The former small difference reflects the small second-order effect of the Pd d orbital mixing on the Pd d peak intensity.

Summary and Conclusions

Pd K-edge XANES spectroscopy probes different molecular orbitals and consequently the charge distribution in a series of (PP)Pd(XX) complexes. The charge redistribution as reflected in the Pd oxidation level is indicated by both the intensity of the Pd d band and the energy of the Pd p band. Further, the increasing covalent interaction between the Pd and coordinated moieties via the Pd p orbitals is directly reflected in the energy splitting seen in the Pd p band.

Figure 11 gives an overview of the different charge distributions possible within (PP)Pd(XX) complexes as a function of the bite angle. The effects of the different charge redistribution mechanisms on the Pd oxidation state are qualitatively shown and summarized in Figure 12 and Table 3. Both the Pd d and Pd p orbitals facilitate the (PP) ligand to Pd and moiety (XX) to Pd charge redistribution, the magnitude strongly depending on the bite angle. Depending on the nature of the coordinating moiety, which determines the interaction with the $[Pd(PP)]^{2+}$ fragment (the latter determined by the bite angle), different amounts of charge redistribution can occur.

For coordinating moieties (XX) with a small covalent interaction within the $[Pd(PP)]^{2+}$ fragment, the charge distribution involves only the metal−ligand system. As shown in Figure 11a, at narrow bite angles, the Pd p and (PP) ligand covalent interaction is large, shifting charge to the Pd. As the bite angle increases, this charge is donated back to the (PP) ligands, making it more ionic in character. Increasing the bite angle further decreases the Pd−(PP) covalent interaction, thereby increasing the effective Pd oxidation state (Figure 12).

For coordinating moieties with a more covalent interaction with the Pd(PP) fragment, the empty Pd $4d_{xz}$ and Pd $5p_z$ orbitals mix with the coordinating moiety and form molecular orbitals. Thus, charge redistribution from the (XX) moiety to the Pd can also take place. Depending on the coordinating moiety (XX), the (XX) moiety to Pd charge redistribution can be facilitated by only the Pd p orbital or by both the Pd p and Pd d orbitals.

In cases where only the molecular orbital consisting of Pd p is occupied (e.g., TCNE), both (PP) ligand to Pd and (XX) moiety to Pd p charge redistributions occur. As shown in Figures 11a, 11b, and 12, the former dominates at narrow bite angle and the latter at wide bite angle. If both the Pd p and Pd d molecular orbitals are filled, the charge redistribution is almost completely dominated by the Pd d charge redistribution. The antibonding interaction between the Pd $4d_{xz}$ and ligand is largest near ∼90°, causing the Pd d orbital to have a maximum in energy at this bite angle as shown in Figures 10 and 11c. The resulting overlap with the coordinating moiety causes the molecular orbital to be mainly located on the allyl, whereas for bite angles narrower and wider than 90° the molecular orbital is mainly located on the Pd. The moiety (XX) to Pd charge

(25) Zuideveld, M. A.; Swennenhuis, B. H. G.; Boele, M. D. K.; Guari, Y.; van Strijdonck, G. P. F.; Reek, J. N. H.; Kamer, P. C. J.; Goubitz, K.; Fraanje, J.; Lutz, M.; Spek, A. L.; van Leeuwen, P. W. N. M. *J. Chem. Soc., Dalton Trans.* **2002**, 2308.

redistribution facilitated by the Pd d produces a maximum in the Pd oxidation state around 90° (Figures 11c and 12).

The total charge rearrangement for (1,1-$(CH_3)_2$−C_3H_3) moiety complexes is less than for (C_3H_5) because of asymmetry in the π orbitals. This asymmetry makes the moiety to Pd redistribution less efficient via the Pd p orbitals. Steric effects may inhibit the covalent interaction at very large bite angles in the (1,1-$(CH_3)_2$−C_3H_3) case.

The allyl complexes, frequently used as catalysts in organic synthesis, show electron density movements from the allyl moiety to the $[(PP)Pd]^{2+}$ fragment with increasing bite angle above 90°. This electron density movement away from the allyl anion activates the allyl moieties for nucleophilic attack. Figures 8 and 10 suggest that the maximum charge on the allyl moieties is present in complexes with the largest bite angles; however, the optimal activity (and selectivity for the (1,1-$(CH_3)_2$−C_3H_3) case) occurs at angles smaller than 110°. This strongly suggests that steric effects, which become larger at increasing bite angles,[12] result in less reactive complexes at large bite angles even though the negative charge on the allyl moiety is still decreasing (enhancing nucleophilic attack). Thus, the optimal bite angle is determined both by electronic and steric effects consistent with previous suggestions in the literature.[7]

The XANES spectroscopy techniques described in this paper can be applied to investigate in principle the molecular orbitals of and charge distributions within every kind of sample. XANES spectroscopy directly probes molecular orbitals. Taking the negative second derivative of these XANES data provides direct information on the energy and charge distribution within the different molecular orbitals probed. The obtained data thus gives essential information about the electronic properties of the sample under investigation. Theoretical ab initio full multiple scattering calculations described in the appendix validate the electronic structure of these Pd complexes and the conclusions drawn.

Appendix

Validation with Theoretical Calculations. Pd K-edge XANES spectroscopy directly probes different unoccupied molecular orbitals in the Pd complexes. Density functional calculations do not approximate the unoccupied molecular orbitals, necessary to properly interpret the XANES data adequately. Therefore, theoretical FEFF8 calculations have been performed, which give an estimate of the absorption spectrum and the DOS for three different $[(PP)Pd(1,1\text{-}(CH_3)_2{-}C_3H_3)]^+$ complexes.

The absorption XANES data and the DOS are calculated for a relatively narrow bite angle complex $[(dppe)Pd(1,1\text{-}(CH_3)_2{-}C_3H_3)]^+$ (86°) and two complexes with wider bite angles $[(dppf)Pd(1,1\text{-}(CH_3)_2{-}C_3H_3)]^+$ (101°) and $[(DPEphos)Pd(1,1\text{-}(CH_3)_2{-}C_3H_3)]^+$ (104°). The negative second derivative is taken for these data as was done with the experimental data and these are shown in Figure 13. The shape of the theoretical negative second derivatives is similar to the experimental data (Figure 2c). A large and small increase in the Pd d peak intensity is observed for the (dppf) ($\beta = 101°$) and the (DPEphos) complexes ($\beta = 104°$), respectively, in comparison to the (dppe) complex ($\beta = 86°$), similar to the experimental data (Figures 13 and 2c). The Pd p peak broadens with increasing bite angle with a simultaneous splitting pattern into two peaks as observed in the experiment data.

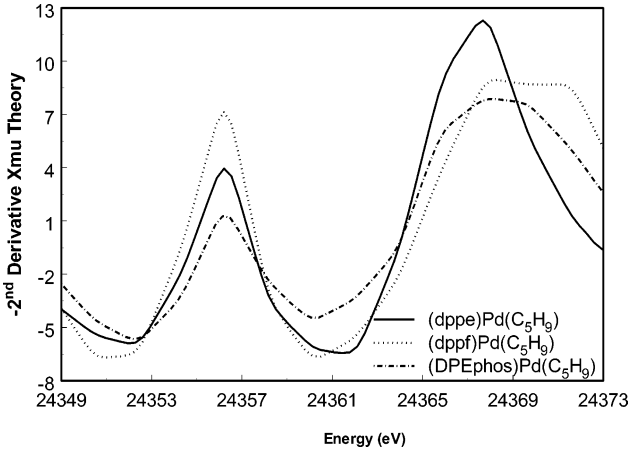

Figure 13. Negative secone derivative of theoretical XANES data for (dppe)Pd(C_5H_9), (dppf)Pd(C_5H_9), and (DPEphos)Pd(C_5H_9) complexes, calculated using FEFF8.0.

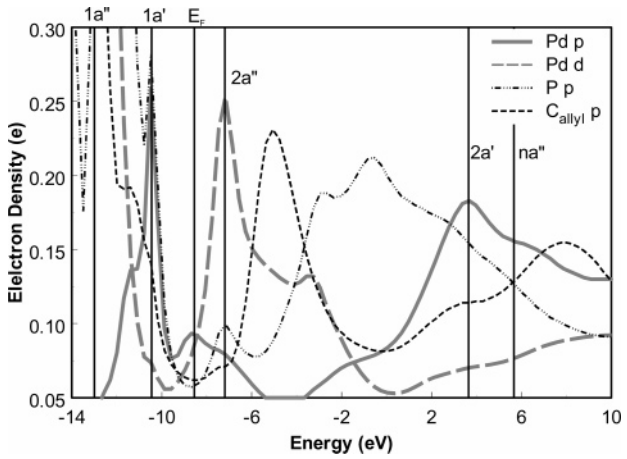

Figure 14. Density of states of the (dppe)Pd(C_5H_9) complex ($\beta = 86°$), calculated using FEFF8.0. The vertical lines (solid black lines) indicate the position of the molecular orbitals.

The Pd d, Pd p, P p, and C_{allyl} p density of states (DOS) for the small bite angle complex $[(dppe)Pd(1,1\text{-}(CH_3)_2{-}C_3H_3)]^+$ are given in Figure 14. FEFF8 calculated a Fermi level (E_F), which is given as a solid line at −8.551 eV. Below this Fermi level, two occupied molecular orbitals are visible which are mainly Pd d and Pd p in character and are assigned as 1a″ and 1a′, respectively. The energy positions of these two molecular orbitals are reversed to the order as was expected on the basis of the orbital interaction diagram (Figure 7a). The empty DOS above this E_F line are probed with Pd K-edge XAS. The first peak in the negative second derivative of the XANES data was assigned as the Pd d peak. This is confirmed by the FEFF8 calculation, showing just above the HOMO a sharp Pd d peak (orbital 2a″) with a Pd p mixing in allowing the Pd p peak to be monitored with Pd K-edge XAS. Additionally, a small shoulder of the C_{allyl} p DOS lines up with this feature, confirming the Pd 4d n_π orbital interaction in this 2a″ MO (Figure 7a). At ∼4 eV, the Pd p peak can be observed, that is, a sharp maximum in the Pd p orbital. This peak (orbital 2a′) is overlapping with the C_{allyl} p DOS as expected on the basis of the orbital interaction diagram (Figure 7a). A third Pd p maximum is observed at ∼6 eV, corresponding to the nonbonding na″ orbital. No alignment with P or C_{allyl} orbitals is observed in this region, consistent with the fact that no overlap

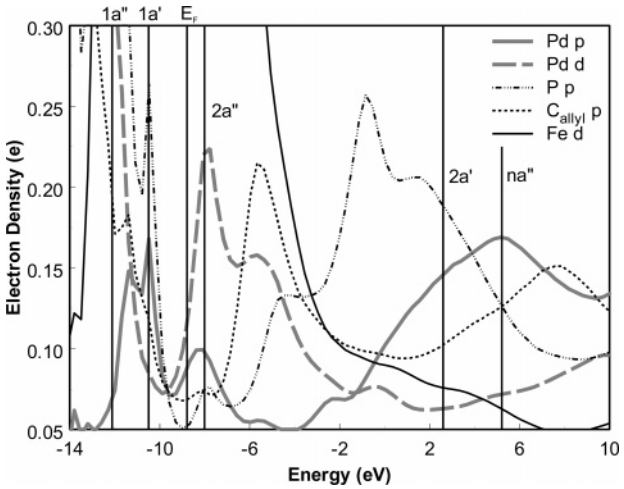

Figure 15. Density of states of the (dppf)Pd(C_5H_9) complex ($\beta = 101°$), calculated using FEFF8.0. The vertical lines (solid black lines) indicate the position of the molecular orbitals.

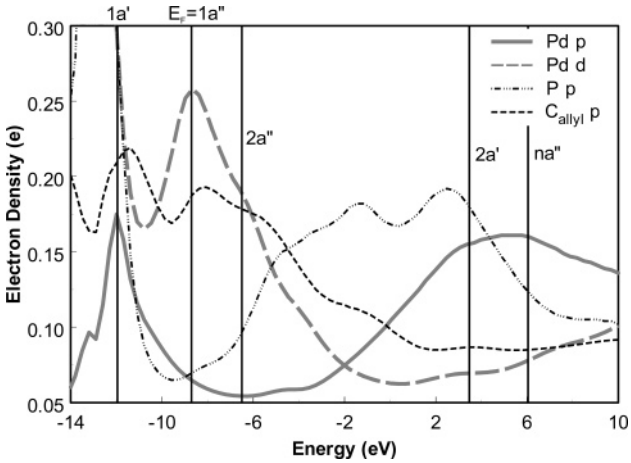

Figure 16. Density of states of the (DPEphos)Pd(C_5H_9) complex ($\beta = 104°$), calculated using FEFF8.0. The vertical lines (solid black lines) indicate the position of the molecular orbitals.

with metal or ligand orbitals takes place for this nonbonding Pd p_y orbital.

The DOS for the [(dppf)Pd(1,1-$(CH_3)_2-C_3H_3$)]$^+$ complexes is shown in Figure 15. The calculated Fermi level is given at −8.788 eV. Again, the order of the two occupied molecular orbitals 1a″ and 1a′ are in contrast to the orbital interaction diagram (Figure 7a). The three XANES absorption peaks are predicted as indicated by the vertical lines. Just above the HOMO level, a Pd d peak with clear amount of Pd p DOS mixing in is evident. Moreover, an enormous Fe d DOS overlapping with the Pd d peak is observed (the electron density is going off scale for the Fe d DOS here). This confirms, as suggested above,[25] that the anomalous high Pd d peak intensity is caused by the presence of the Fe atom. Although the Fe atom is located at a distance of ∼4 Å to the Pd absorber atom, the radial extend of the Fe d orbital is large enough to mix in with the Pd d. In the range of ∼−1 to 9 eV, a relatively broad Pd p peak can be observed. This Pd p peak is lining up with the C_{allyl} p at ∼3 eV confirming this as the 2a′ molecular orbital. The maximum at ∼5.5 eV is assigned to the na″ molecular orbital.

In Figure 16, the DOS of the [(DPEphos)Pd(1,1-$(CH_3)_2-C_3H_3$)]$^+$ is displayed. The Fermi level is calculated at −8.910 eV, which is exactly at the occupied 1a″ molecular orbital. The occupied 1a′ molecular orbital, which is mainly Pp p in character, is now found at lower energy than the HOMO 1a″, consistent with the orbital interaction diagram. The three absorption peaks are predicted. A large overlap from the Pd d peak with C_{allyl} p is indicated, as expected for these large bite angle complexes (Figure 11). From ∼3 until ∼7 eV a broad Pd p peak is indicated, which is at ∼3.5 eV lining up with the C_{allyl} p indicating this is the 2a′ orbital and at the maximum around ∼6 eV from the na″ orbital.

In conclusion, although the experimental and modeled XAFS results are not identical, the general trends found for the [(PP)-Pd(allyl)]$^+$ complexes are similar. The self-consistent field muffin-tin approximation made in FEFF8 is not fully adequate for charge-transfer complexes such as those studied here. Moreover, as FEFF8 is developed to calculate the unoccupied molecular orbitals, it may predict the bonding orbitals wrongly. It is therefore not surprising that FEFF8 does not predict all the different charge redistribution effects (including the occupied molecular orbitals 1a′ and 1a″ for these complexes) perfectly well. However, FEFF8 does predict the proper general trends and helps us interpret and assign the different molecular orbitals observed in the experimental data.

Supporting Information Available: Normalized Pd K-edge XANES spectra of series of bidentate diphosphine ligand palladium complexes with a series of bite angles. This material is available free of charge via the Internet at http://pubs.acs.org.

JA048225N